Experimental demonstration of fiber-accessible metal nanoparticle plasmon waveguides for planar energy guiding and sensing

Stefan A. Maier,[a] Michelle D. Friedman, Paul E. Barclay, and Oskar Painter
Thomas J. Watson Laboratory of Applied Physics, California Institute of Technology, Pasadena, California 91125

(Received 12 April 2004; accepted 12 December 2004; published online 7 February 2005)

Experimental evidence of mode-selective evanescent power coupling at telecommunication frequencies with efficiencies up to 75% from a tapered optical fiber to a metal nanoparticle plasmon waveguide is presented. The waveguide consists of a two-dimensional square lattice of lithographically defined Au nanoparticles on an optically thin silicon membrane. The dispersion and attenuation properties of the waveguide are analyzed using the fiber taper. The high efficiency of power transfer into these waveguides solves the coupling problem between conventional optics and plasmonic devices and could lead to the development of highly efficient plasmonic sensors and optical switches. © *2005 American Institute of Physics*. [DOI: 10.1063/1.1862340]

Micro- and nanostructured assemblies of metals sustaining coherent, nonradiative electronic excitations known as surface plasmon polaritons[1] are an intriguing materials system promising a wide range of applications in photonics and telecommunications.[2] Basic building blocks of plasmonic devices will be planar metallic waveguides such as micron-sized stripes,[3] nanowires,[4] and nanoparticle arrays[5] for the transport of electromagnetic energy with a mode confinement on wavelength and subwavelength scales. However, the excitation of spatially localized plasmons in such waveguides poses a considerable challenge due to the small size and complex mode shape of the guided modes, resulting in a huge spatial mismatch with diffraction-limited optical beams and conventional waveguides. For far-field excitation of localized plasmons in thin Au films, coupling efficiencies of about 15% have been estimated,[6] while the excitation of subwavelength-scale modes in one-dimensional (1D) nanoparticle waveguides typically employs near-field fiber probes with light throughputs below 0.1%.[7] Moreover, neither of the two methods is mode selective. Using a recently developed design concept[8] for metal nanoparticle plasmon waveguides based on silicon-on-insulator (SOI) technology, we present experimental observations of mode-selective energy transfer in the 1500 nm wavelength band from a conventional fiber taper to a plasmon waveguide with efficiencies up to 75%. This concept is extendable to higher frequencies and promises applications in energy guiding and optical sensing with high efficiencies.

The demonstration of non-diffraction-limited guiding of electromagnetic energy over micron- and submicron distances in resonantly excited metallic nanowires[4] and nanoparticle waveguides[5] has recently been achieved as a first step towards the ultimate goal of building highly integrated photonic circuits for channeling energy to nanoscale detectors. Due to the heightened local fields surrounding metallic guiding structures, such devices could find useful applications not only in photonics and telecommunications but also in biological sensing[9] of molecules in localized "hot spots." For this vision to come true, new ways of coupling light into such devices have to be developed that are more efficient than non-mode-selective techniques such as diffraction-limited far-field coupling and local excitation using nanoscopic probes. On a larger scale, the nonresonant guiding of electromagnetic energy at visible[10] and near-infrared frequencies[3,11] using micron-scale metallic stripes has been demonstrated over distances up to several hundred microns employing far-field and end-fire excitation techniques, respectively. However, such long-ranging surface plasmon polaritons can only be sustained and efficiently excited for stripes embedded in a symmetric environment,[12] making them of limited use for sensing applications and also complicating the employment of these structures as input ports to sub-diffraction-limit plasmon waveguides.

To overcome this challenging obstacle, we have developed a design concept of a metal nanoparticle plasmon waveguide[8] that can be efficiently excited via evanescent, phase-matched coupling using small tapers drawn from standard silica fibers.[13,14] The waveguide consists of a hybrid structure of SOI and a lithographically defined square lattice of metal nanoparticles on an optically thin, undercut silicon membrane. In order to allow for nonresonant excitation of the metal nanoparticles to reduce the absorptive heating losses without a concomitant increase in radiative loss, we employ a lateral grading in nanoparticle size to confine the mode to the center of the waveguide (note that for 1D metal nanoparticle chains, resonant excitation with significantly higher heating losses is necessary[15] in order to tightly confine the mode to the subwavelength guiding structure). Vertically, the confinement is ensured both by bound metal/air surface plasmons and the undercut geometry of the silicon membrane. Figure 1(a) shows an example of a finite-difference time-domain (FDTD) calculated optical mode profile (electric field intensity) for the fundamental waveguide mode in top and side geometry.

Due to the periodicity of the structure in the propagation direction, the dispersion relation of the plasmon polariton modes is folded back into the first Brillouin zone. This way, the upper plasmon band crosses both the light-lines of silica and air, suggesting the possibility of phase-matched, mode-selective excitations of the waveguide using silica fiber tapers[14] placed in close proximity to the waveguide. In order

[a]Present address: Department of Physics, University of Bath, UK; electronic mail: S.Maier@bath.ac.uk

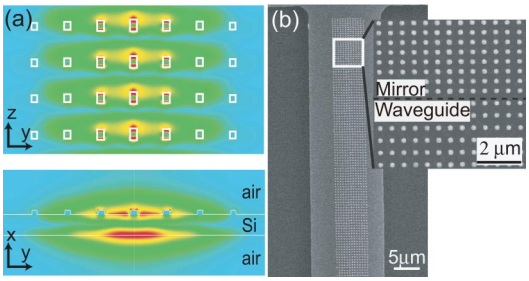

FIG. 1. (Color online) (a) Electric field intensity distribution of a plasmon waveguide mode in top (upper plot) and side view (lower plot) calculated using FDTD simulations. (b) Scanning electron micrograph of a fabricated plasmon waveguide on an undercut Si membrane. The waveguide is terminated by mirrors at both ends.

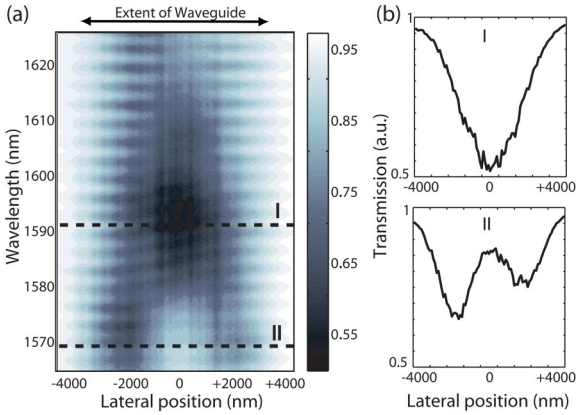

FIG. 2. (Color online) (a) Contour plot showing the transmitted power through the fiber taper on a linear color scale versus wavelength and lateral position of the taper with respect to the waveguide. (b) Lateral transmission profile at a wavelength of 1590 nm (fundamental mode, upper graph) and 1570 nm (higher order mode, lower graph).

to spatially and spectrally investigate energy transfer in this system, we fabricated a plasmon waveguide designed to allow efficient evanescent coupling with a fiber taper at a wavelength of 1.6 μm in the telecommunication band. Figure 1(b) shows scanning electron micrographs of the fabricated waveguide based upon a 530 nm square lattice of Au nanoparticles on a 250 nm Si membrane created by undercutting the 2 μm silica layer of a SOI wafer using hydrofluoric acid. The nanoparticles are 50 nm in height, and have a diameter of approximately 250 nm in the center of the waveguide, with a linear lateral grading down to 210 nm after three of the six lateral periods.

The waveguide is terminated by mirrors consisting of a short (20 period) plasmon waveguide section with a compressed lattice, which is designed to shift the phase-matched waveguide mode into the one-dimensional (1D) band gap of the mirror section.[16] The mirror waveguide section is abruptly ended, and an approximately 10 μm gap then exists from the end of the mirror to the etched facet interface between the silicon slab and the surrounding air.[17]

A fiber taper of minimum diameter $\sim$1.5 μm was fabricated and spliced into a fiber line containing a fiber-coupled swept wavelength laser source ($\lambda = 1565-1625$ nm) at its input and a photodetector at its output for measuring the transmitted signal. The fiber taper was mounted in a U-shaped configuration and positioned using a set of *x*-*y*-*z* stages with 50 nm encoder resolution. Details of the mounting and positioning methods for the fiber taper can be found in Ref. 17. The taper was carefully aligned along the axis of the plasmon waveguide and parallel to the surface of the Si chip. At a taper height of several microns above the center of the waveguide, the taper mode did not interact with the waveguide, resulting in unity transmission over the entire wavelength range. The taper was then slowly brought into the near field of the plasmon waveguide until a resonant drop in transmission indicative of coupling to the plasmon waveguide was observed. Lateral movement of the taper at constant height allowed then the examination of the spatial coupling profile. Figure 2(a) shows a contour plot of the power transmitted through the fiber taper on a linear color scale versus wavelength and lateral taper position. Several spectral and spatial features are clearly discernible. When the taper is shifted completely off the waveguide, the transmission through the taper is almost unity but for direct coupling into the thin Si support membrane, evidenced by a broadband periodic signal modulation of small amplitude caused by Fabry–Perot resonances (period 3.2 nm) from reflections at the etched facet ends of the 130-μm-long silicon membrane (effective index 2.85). Over the outer parts of the waveguide, the period of this modulation stays constant, while its amplitude increases, which we attribute to enhanced coupling into the silicon slab mediated by the metal nanoparticle lattice. As the fiber taper is moved to the center of the waveguide, a strong resonant dip in taper transmission centered around a wavelength of 1590 nm is observed, indicative of resonant coupling to the fundamental plasmon waveguide mode. Although much weaker in strength, for the taper near the outer edges of the waveguide (on both sides), a resonance dip around a wavelength of 1570 nm is also discernable in the transmission data. We believe this resonance around 1570 nm to be due to excitation of the first higher-order odd plasmon waveguide mode, in good agreement with predictions from FDTD simulations (see EPAPS Ref. 18). Fig. 2(b) summarizes these results by showing the lateral transmission profile at wavelengths 1590 nm (fundamental resonance, upper graph) and 1570 nm (higher-order mode resonance, lower graph). The measured spatial full width at half-maximum of $\sim$4 μm of the fundamental mode is rather large, even after taking into account convolution effects with the finite width of the fiber taper. We attribute this to the broadband loss from the metal-assisted scattering discussed earlier which tends to accentuate the tails of the lateral profile. Different depths of the transmission profile on either side of the waveguide are also visible [see lower graph of Fig. 2(b)], which may be due to small height variations during lateral movement of the taper and/or actual fabrication nonidealities of the waveguide.

The dispersion of the fundamental mode was further examined by translating the fiber in the direction of the waveguide in steps of 200 μm, thereby varying the fiber diameter and thus the wave vector of phase matching. Figure 3(a) shows the spectral position of the transmission minimum corresponding to resonant coupling to the fundamental plasmon waveguide mode versus taper position along the waveguide direction. The point of minimum fiber diameter [$x=0$ in Fig. 3(a)] was determined optically. A careful analysis of the fiber profile was not performed here, as was done in Ref. 17, since only the general trend in the fiber diameter is of interest. The redshift of the resonant coupling with increasing fiber diameter is indicative of contradirectional

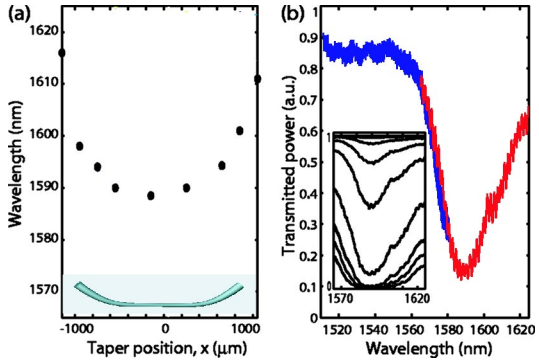

FIG. 3. (Color online) (a) Plot of the resonant transmission minimum due to coupling to the fundamental plasmon waveguide mode versus coupling position along the fiber taper. $x=0$ corresponds to the position of minimum taper diameter, and for larger taper diameters the resonant coupling wavelength is seen to redshift, indicative of contradirectional coupling from the fiber taper to the plasmon waveguide (see Ref. 17). (b) Wavelength scan of the transmitted power through the fiber taper placed in close proximity over the centre of the plasmon waveguide obtained using two different external cavity lasers with overlapping scan ranges. The inset shows the evolution of the coupling when the taper is successively lowered towards the waveguide in 50 nm steps (every tenth step shown).

coupling,[17] strong evidence that phase matching is indeed taking place between the zone-folded upper plasmon band and the fundamental fiber taper mode.

The efficiency of power transfer into the fundamental plasmon waveguide mode was studied using a newly drawn fiber taper of 1.1 μm diameter. Figure 3(b) shows a representative wavelength scan of the transmitted signal at a height of ~ 1 μm above the waveguide center. For this height, the normalized transmitted signal dropped to 0.12 at the center of the resonance dip, while recovering back to 0.75 at the higher frequency end of the laser scan range (red curve). Using a second laser with a scan range between 1510 and 1580 nm, a nearly complete recovery of the transmission to about 0.87 was confirmed (blue curve). We have thus observed a power transfer of about 75% from the fiber taper to the plasmon waveguide.[16]

In all our experiments, the depth of the resonance dip in transmission was seen to increase monotonically with decreasing taper height as expected for contradirectional coupling (i.e., no Rabi-type flopping of power as in codirectional coupling). The inset of Figure 3(b) shows examples of wavelength scans of the transmitted power for different taper heights, decreasing from 4 μm to zero gap (defined as the gap where taper is touching the surface) in 500 nm steps. Note that the wavelength dependence of the coupling is broader and not as sharply defined as in an ideal contradirectional coupler, which we believe to be due to fabrication nonidealities.

The occurrence of Fabry–Perot resonance features in the transmission data of Fig. 3(b) [of different period than the modulations due to Si slab coupling discussed in conjunction with Fig. 2(a)] allowed the estimation of the group velocity and energy decay length of the propagating plasmon mode. By analyzing the spacing and width of the resonances, the group velocity was thus estimated to about 15% of the velocity of light in vacuum (corresponding to a group index of 6.67), in good agreement with FDTD simulations,[8] and the $1/e$ energy decay length to about 50 μm. Note that the decay length estimate assumes perfect mirror reflectivities, and as such 50 μm is a lower estimate of the actual decay length.

At this point, it is worth noting that our design concept can also be scaled to higher frequencies towards the visible regime of the spectrum by an appropriate change in lattice constant. The higher absorptive losses for near-resonant excitations at lower wavelengths can then be partially counteracted by a change of the materials system to silver. The high efficiency of power transfer into our plasmon waveguide should thus allow intriguing applications at visible and near-infrared frequencies. For example, the use as a coupling structure to other planar plasmonic devices such as cavities and resonantly excited 1D particle waveguides as presented in Ref. 5 can be envisioned. Moreover, the accessibility of the optical surface mode suggests it is promising for the optical sensing of biological agents as well.

In summary, we have presented a plasmon waveguide based on a two-dimensional lattice of Au nanoparticles on a thin silicon membrane fabricated using SOI processing techniques that can be efficiently excited using fiber tapers. Mode-selective power transfer efficiencies up to 75% have been demonstrated. Such waveguides could make possible the interconnection of a wealth of recently proposed plasmonic micro- and nanostructures with conventional fiber optics and also lead to the design of high-performance plasmonic sensors.

The authors are grateful to M. Borselli and T. J. Johnson for help with fabrication.

[1] H. Raether, *Surface Plasmons on Smooth and Rough Surfaces and on Gratings* (Springer, Berlin, 1988).
[2] W. L. Barnes, A. Dereux, and T. W. Ebbesen, Nature (London) **424**, 824 (2003).
[3] R. Charbonneau, P. Berini, E. Berolo, and E. Lisicka-Shrzek, Opt. Lett. **25**, 844 (2000).
[4] J. R. Krenn, B. Lamprecht, H. Ditlbacher, G. Schider, M. Salerno, A. Leitner, and F. R. Aussenegg, Europhys. Lett. **60**, 663 (2002).
[5] S. A. Maier, P. G. Kik, H. A. Atwater, S. Meltzer, E. Harel, B. E. Koel, and A. A. G. Requicha, Nat. Mater. **2**, 229 (2003).
[6] H. Ditlbacher, J. R. Krenn, A. Hohenau, A. Leitner, and F. R. Aussenegg, Appl. Phys. Lett. **83**, 3665 (2003).
[7] D. Courjon and C. Bainier, Rep. Prog. Phys. **57**, 989 (1994).
[8] S. A. Maier, P. E. Barclay, T. J. Johnson, M. D. Friedman, and O. Painter, Appl. Phys. Lett. **84**, 3990 (2004).
[9] G. Raschke, S. Kowarik, T. Franzl, C. Sönnichsen, T. A. Klar, J. Feldmann, A. Nichtl, and K. Kürzinger, Nano Lett. **3**, 935 (2003).
[10] B. Lamprecht, J. R. Krenn, G. Schider, H. Ditlbacher, M. Salerno, N. Felidj, A. Leitner, F. R. Aussenegg, and J. C. Weeber, Appl. Phys. Lett. **79**, 51 (2001).
[11] T. Nikolajsen, K. Leosson, I. Salakhutdinov, and S. I. Bozhevolnyi, Appl. Phys. Lett. **82**, 668 (2003).
[12] P. Berini, Phys. Rev. B **63**, 125417 (2001).
[13] M. Cai, O. Painter, and K. J. Vahala, Phys. Rev. Lett. **85**, 74 (2000).
[14] P. E. Barclay, K. Srinivasan, M. Borselli, and O. Painter, Electron. Lett. **39**, 842 (2003).
[15] S. A. Maier, P. G. Kik, and H. A. Atwater, Phys. Rev. B **67**, 205402 (2003).
[16] P. E. Barclay, K. Srinivasan, M. Borselli, and O. Painter, Opt. Lett. **29**, 697 (2004).
[17] P. E. Barclay, K. Srinivasan, M. Borselli, and O. Painter, Appl. Phys. Lett. **85**, 4 (2004).
[18] See EPAPS Document No. E-APPLAB-86-076506 for a FDTD-calculated mode profile of the first higher order mode. A direct link to this document may be found in the online article's HTML reference section. The document may also be reached via the EPAPS homepage (http://www.aip.org/pubservs/epaps.html) or from ftp.aip.org in the directory /epaps/. See the EPAPS homepage for more information.